Transition metal complex as optical probes for super resolution microscopy

Sumit Kumar Pramanik[1], Sreejesh Sreedharan[2], Noufal Kandoth[3], Amitava Das,[3†] and Jim A Thomas.[4†]

[1] CSIR-Central Salt and Marine Chemicals Research Institute, Bhavnagar, Gujarat, India

[2] College of Science and Engineering, University of Derby, Derby, DE22 1GB, UK

[3] Indian Institute of Science Education and Research Kolkata, Mohanpur 741246, West Bengal, India.

[4] Department of Chemistry, University of Sheffield, Sheffield, S3 7HF, UK

[†]e-mail: amitava@iiserkol.ac.in; james.thomas@sheffield.ac.uk

Abstract | The suite of techniques encompassing optical super-resolution microscopy (SRM) can facilitate detailed visualization of biological structures and biochemical transformations at unprecedented levels of resolution and contrast; however, they depend on imaging probes with specific biophysical and photophysical properties. In this context, metal complexes with tunable photo-excited states and stability towards photobleaching are promising candidates for advanced imaging techniques. This review illustrates how, by selecting appropriate optical properties and luminescence responses, metal complexes can be utilized as probes for a range of SRM techniques including multimodal imaging to study subcellular architecture and dynamics with nanoscale resolution. Limitations and challenges of the existing molecular probes are also discussed. By highlighting these recent innovations and providing suggestions for future directions, this review further underscores the importance of optical probes in pushing the boundaries of SR microscopy and advancing our understanding of complex biological systems.

Introduction

Confocal laser scanning fluorescence microscopy (CLSM) is one of the most important tools for real-time visualizing of cellular structures and intracellular metabolic processes in live cells. This non-invasive technique has significantly contributed to the developments of cell and chemical biology over the last few decades. [1-3] Yet, the spatial resolution of fluorescence microscopy is restricted by the Abbe diffraction limit ($R_{Lateral} \approx \lambda/2NA$, where R is spatial resolution λ is the average wavelength of illumination in the excitation wavelength band in fluorescence, *NA* is the numerical aperture of the optical system). [4-8] This implies that for a typical confocal fluorescence microscope operating in the visible spectrum, the smallest object that can be resolved by optical microscopy is limited to ≥ 200 nm. [5] Furthermore, for 3D images, the Rayleigh criterion restricts resolutions along the optical axis to $R_{Axial} \approx \lambda/2NA^2$.[9]

To address these issues, several approaches to SRM have been developed that achieve sub-diffraction-limit resolution both in the lateral and axial direction, improving the resolution capabilities of fluorescence imaging in the nanoscale regime. These techniques can provide multi-colour, multidimensional, and dynamic information on biomolecules within living specimens at spatial resolutions < 10 nm. [5,9]

Box 1 General Considerations for the Choice of the Luminophore in SRM:

The nature of the luminophores used for SRM is crucial in achieving desired outcomes. For example, the 5-fold higher spatial resolution accomplished by stimulated emission depletion (STED) requires a luminophore that can survive at least 25 on-off switching cycles under irradiation with a depletion intensity that is approximately 25 times higher than the characteristic saturation intensity of a luminophore in conventional CLSM use.[10-12] Higher switching cycles reduce the scanning step size and enhance Nyquist resolution. Luminophores that are resistant to photobleaching permit higher depletion intensities promoting better spatial resolution and extended observation times.[13] Furthermore, the stimulated emission cross-section of a luminophore, its intersystem crossing rate, and the cross-section of light-induced transition to a non-emissive state are important parameters for the off-switching rate, which is crucial to STED, ground state depletion (GSD), reversible saturable optical transition (RESOLFT) and structured illumination microscopic (SIM) approaches.[14] Luminophores that can achieve better Nyquist resolution in single-molecule localization microscopic (SMLM) techniques require lower fluorescence on-off duty cycle values. This helps to minimize overlap between stochastically activated luminophores, promoting high localization densities and improved resolution. [15,16] Thus, although resistance towards photobleaching and off-switching transition rates are crucial parameters for most super-resolution techniques, different techniques have varying requirements in terms of the balance of non-emissive states and off-switching transition properties. Consequently, a rationalized choice of luminophores must be made for each technique.[17-20] In fact, as new super-resolution microscopy technologies become available, one of the crucial limiting factors for exploring their full live-cell imaging is the availability of appropriate luminescent probes. [21-28] In this context, synthetic organic molecules are typically a popular choice owing to their facile functionalization, smaller sizes, and the perceived appropriate lipophilicity balance for cell membrane permeability. [11,29-34] However, such organic fluorophores typically suffer from issues around narrow Stokes shifts, short luminescence lifetimes, shorter wavelength luminescence maximum, and photobleaching/ photodegradation. [35] A range of purpose-built semiconductor quantum dots (QDs), up-conversion nanocrystals (UCNPs), polymer dots (PDs), and graphene QDs have also been explored for use as an imaging probe. Despite having favorable optical properties for imaging applications, their uncertain surface biochemistry and systemic toxicity towards human physiology have limited their use in real-time applications.[36] The typical stability of transition metal complexes towards photobleaching, along with their tunable optical properties are ideally suited to address these issues. Despite such advantages, their usage in SRM is still in its infancy. Nevertheless, with the expanding options for SRM techniques, the use of transition metal complexes in this area is rapidly developing and, as this review illustrates, in many ways they are ideally suited for such applications.

A common consideration for any probe used in live cell microscopy or SRM techniques is its toxicity, with phototoxicity being particularly relevant. By definition, the excited states of molecules are more energetic and hence more reactive than their ground state. Commonly, photobleaching of a probe is a cause of phototoxicity due to photoactivation of reactive oxygen

species, ROS.[37-39] This typically occurs through two possible mechanisms; in Type I reactions, ROS such as superoxide, peroxides, and hydroxyl radicals are generated through direct redox reactions with a photoexcited probe. In a Type II process, the triplet state of the probe generates the ROS singlet oxygen through an energy transfer process. [40,41] Such processes are exploited in Photodynamic therapy, PDT. However, for PDT applications a higher-power laser source and a photosensitizer with a high-energy excited state that can efficiently generate ROS are selected. [42,43] In optical bio-imaging, Type I and II processes are minimized by a combination of less intense laser sources and lowered probe concentrations. However, these conditions require brightly emissive probes with relatively low emission energies which will decrease the efficiency of ROS generation.[44] Probes with lowered excitation energies offers a second advantage as biological tissue is more transparent to deep red and near-infrared wavelengths.

Box 2 | The potential of polypyridyl d^6 transition metal complexes

The potential of metal complexes to address the issues discussed in Box 1 are exemplified by hexacoordinated second/third-row transition metal complexes having D_3 symmetry and nd^6 electronic configuration – see Fig 1 for examples of structures discussed in this report. These metal ions form low-spin diamagnetic complexes with coordinating ligands like N∧N (2,2'-bipyridyl / 1,10-phenanthroline and derivatives), N∧C (2-phenyl pyridine) that are generally kinetically inert in their ground and photoexcited states. Indeed, among such complexes, Ru(II)-polypyridine ($Ru(N\wedge N)_3^{2+}$ and cyclometalated Ir(III) complexes ($Ir(N\wedge C)_2(N\wedge N)^+$ have received significant attention across a range of applications that exploit these distinctive and rich photophysical properties.[45-52] Typically, such complexes are stable towards substitution reactions in aqueous buffer medium and also in biofluids. Their high absorptivity and luminescence quantum yields mean they can be used at minimal concentrations for imaging applications, reducing any disruptive effects to biological processes in live cells. Furthermore, as they generally display long lifetime and luminescence maxima beyond 550 nm, the possibility of interference from endogenous fluorophores is minimized.

These complexes have a characteristic metal-to-ligand charge-transfer, MLCT, transition band in the visible region with high molar absorptivity (ε) (~ 10^4 $M^{-1}cm^{-1}$). [53,54] This excitation generally results in effective population of a singlet state (^{1}S: ^{1}MLCT), which subsequently undergoes an efficient (Φ_{ISC} ~ 1.0) intersystem crossing (ISC) to populate the ^{3}MLCT excited state. The ISC process is associated with a large Stoke shift (> 100 nm), so that emission occurs at significantly longer wavelengths and minimizes inner filter effects. For Ru(II)-polypyridyl complexes a relatively long lifetime (~ 250 ns in aq. medium saturated with dissolved O_2) is observed for ^{3}MLCT based emission at ~ 600 nm. [55] While $Ir(N\wedge C)_2(N\wedge N)^+$ complexes show a strong vibrationally structured luminescence band having a maximum around ~ 710 - 725 nm that is assigned to a mixed excited state with a large MLCT-based contribution. Typically, such complexes show a slightly shorter luminescence lifetime compared to their Ru(II) analogues (~100 ns in aerated aq. solution). [54,56-58]

Metal complexes and SRM: photophysical considerations

It has been established that the long emission lifetimes of complexes such as polypyridyl d^6 metal complexes are exploitable in lifetime imaging microscopy. Although this is commonly labelled as fluorescence lifetime imaging microscopy (FLIM), it is formally *phosphorescence* lifetime imaging microscopy (PLIM). [59,60] FLIM/PLIM not only allows the facile differentiation of long-lived emission signals from relatively short-lived autofluorescence and light scattering but also enables multiplex imaging. [61,62] However, as outlined in Box 1 and 2, properties such as the high photostability of these complexes render them promising candidates for several SRM modalities; [4,63] a case in point being provided by a consideration of the ideal properties of a STED probe. [64,65]

The lateral resolution ($R_{Lateral}$) of STED nanoscopy is linked to I_{max} (peak intensity of the STED laser) and I_{satu} (STED laser threshold Intensity that results in 50% depletion of the emission intensity of the probe molecule) through Eq. 1:

$$R_{\text{Lateral}} = l\left(1 + \frac{I\text{max}}{I\ \text{sat}}\right)^{-0.5}$$

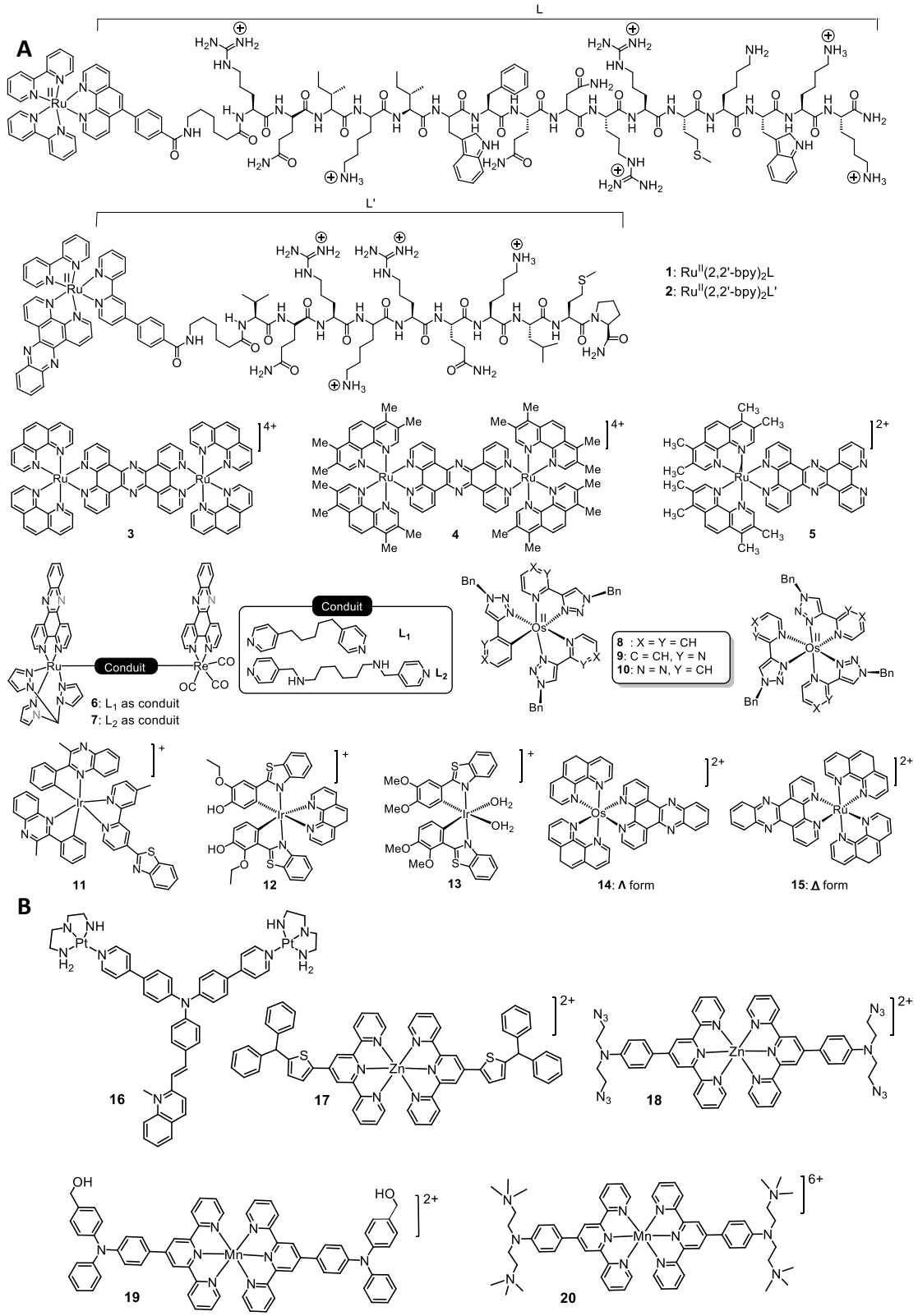

Figure 1| **Molecular structures of metal ion complexes utilized for SRM discussed in this review article** A Molecular structure of polypyridyl d^6 *metal* ion complexes. B. Molecular structures for other luminescent transition metal complexes.

Taken together, the criteria discussed above suggest that the optical properties of an ideal molecular probe for STED microscopy should exhibit good photostability, a long-lived emissive state with a high-intensity red-to-NIR emission spectrum, and also display an overlap of its emission spectrum with the STED depletion beam while avoiding re-excitation through ground state absorbance. On top of these optical properties, for any probe to be exploited for intracellular or in-vivo imaging applications, it should be physiologically benign and display cell membrane permeability and organelle/tissue specificity. [66,67] Facile functionalization of coordinating ligands in such complexes not only offers the option to modulate their optical properties but, can also be used to create luminophores that specifically bind to targeted organelles or structures. Complexes that exhibit chemiluminescence are also highly attractive for *in vivo* imaging; as this emission process does not require an excitation source it negates the interference caused by autofluorescence and offers a much higher signal-to-noise ratio. [68-70] In what follows, we outline the potential of these systems as SRM probes as illustrated by selected recent reports.

Ruthenium(II) complexes as probes and theragnostics

In 2016, the Keyes group reported on two organelle-targeting STED probes, complexes **1** and **2**, which they found to be suitable for both continuous wave and time-gated STED organelle imaging. [71] In this work, the authors exploited the properties of signal peptide to precisely target intracellular localities or organelles. As shown in Fig 2, organelle-specific imaging was accomplished by coordinating two different phenanthroline-peptide conjugates to a Ru^{II}-moiety to yield endoplasmic reticulum (**1**) and nuclear targeting (**2**) probes.

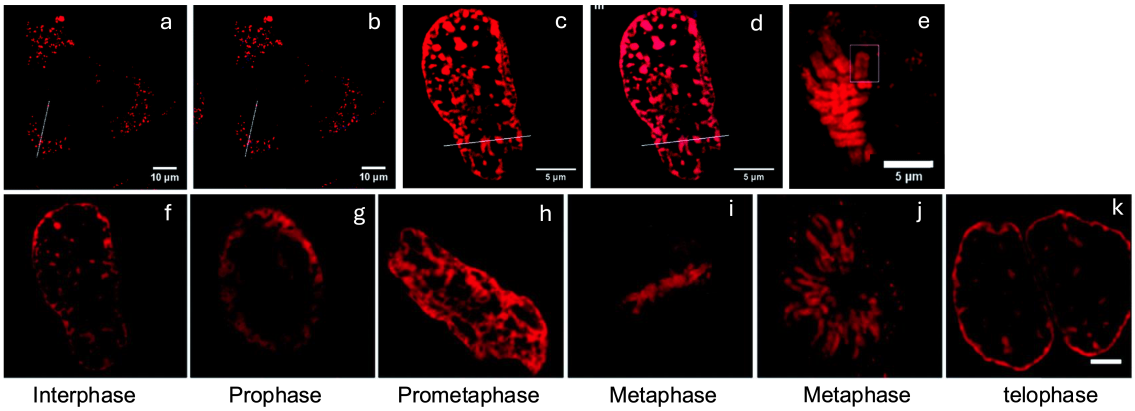

Figure 2| **CLSM and STED nanoscopy using Ru^{II}-based organelle-targeting probes** (a)-(d) CLSM images of live HeLa cells: (a) **1** in ER, (b) merged image of **1** with ER blue, (c) **2** in nucleus, (d) merged image of **2** with DAPI. (e) STED images of **2** bound to chromosomal DNA in the nucleus during metaphase. (f)-(k) STED images using complex **2** to show the different stages of cell division in fixed HeLa cells. Reprinted with permission from ref. 71, Royal Society of Chemistry.

In related work, the Thomas group and collaborators reported a cell-permeant heteroleptic dinuclear Ru(II)-polypyridyl complex, **3**, that binds nuclear DNA ($K_b > 10^7\ M^{-1}$) and stains chromatin. Early studies showed luminescence in the near-infrared (NIR) wavelengths and were used to image nuclear DNA within live cell nuclei. Subsequently, the long lifetime of the DNA-bound probe could be exploited for lifetime imaging microscopy (Fig. 3) using a two-photon absorbance regime

in which FLIM was used to image nuclear DNA in live MCF-7 cells. [72] When the complex was used in fixed cells it showed a luminescence lifetime of ~ 160 ns within the nucleus and a shorter lifetime within the cytoplasm providing imaging with higher sensitivity without interference from intracellular luminescence.[73]

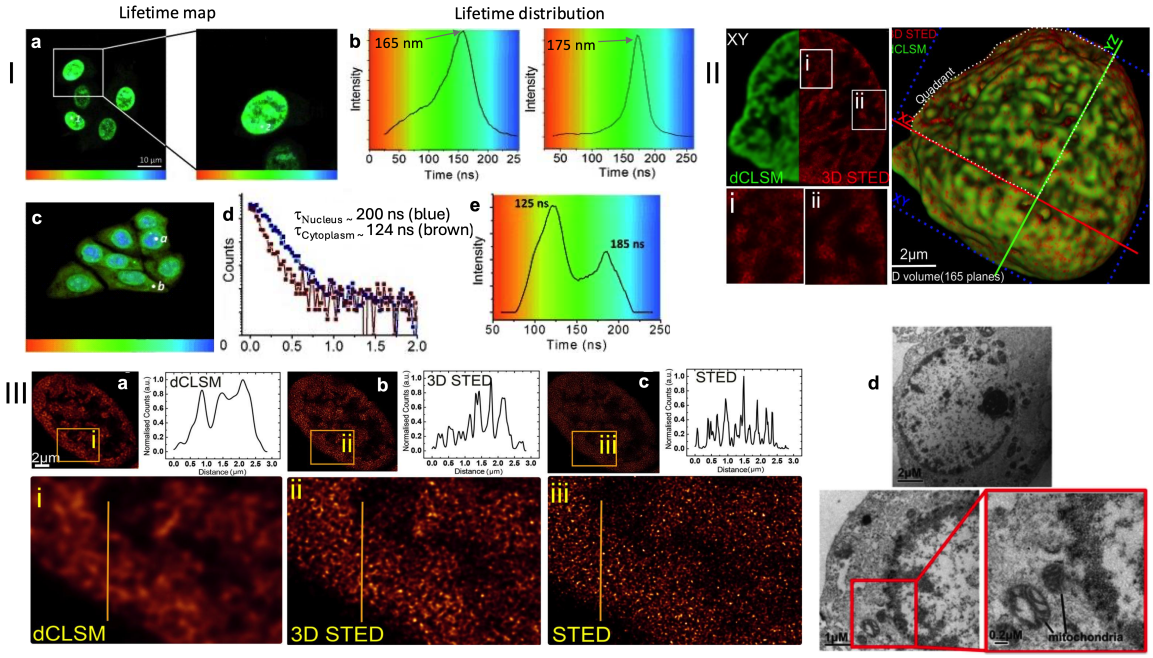

Figure 3| **Multiple imaging modalities of Ru^{II}-complex 3**. (I) Two-photon phosphorescence lifetime imaging of live MCF-7 cells pre-treated with complex **3** in serum-free media with (a) lifetime mapping and (b) distribution, respectively. In both (a) and (b) lifetime data in a single cell is shown to the right. (c) 2P-PLIM imaging using **3** in fixed permeabilized MCF7 cells (d) corresponding emission decay (e) corresponding lifetime distribution. (II) Left: 3D HyVolution (dCLSM) and 3D-STED comparison for XY plane of a single fixed MCF7 cell treated with **3** (the white squared insets are magnified below the images) Right: 3D-STED super-resolved reconstruction of the whole nucleus volume (full 3D volume from 165 planes), where each single plane was imaged at the highest X, Y, and Z STED resolution (3D-STED). Merged dCLSM and STED reconstructed 3D surface rendered images in green and red colour, respectively. (III) Images of live cell staining with **3**. HyVolution (dCLSM) (a), 3D-STED (b), and STED (c); (i–iii) magnified images yellow boxes a, b, and c, respectively. (d) TEM images of the localization of **3** (as contrast agent) (500 µM) in the nucleus and mitochondria of an MCF7 cell. Reprinted with permission from ref. 72 and 73. Parts (I) adapted with permission from ref. 72, Wiley. Part (II) and (III) reprinted with permission from ref. 73, American Chemical Society.

More detailed follow-on studies on the SRM/multimodal imaging capabilities of **3** revealed that at low concentrations it solely localizes in mitochondria and it is only at higher concentrations that localization in the nucleus occurs. In associated STED experiments, the large Stokes shifts (~170 nm) of complex **3** provided excellent matching to a 775 nm depletion line, which avoids anti-Stokes excitation. Its long lifetime when bound to biomolecules facilitated its use in gated STED-Fig 3 II(a-c), where its performance was found to be superior to the commonly used dye, AlexaFluor, which displays more pronounced photobleaching and a narrow Stokes's shift. As it

incorporates two electron-dense Ru^{II} -metal centers, complex **3** is also a contrast agent for DNA in transmission electron microscopy (TEM) (Fig. 3 III-d). [73]

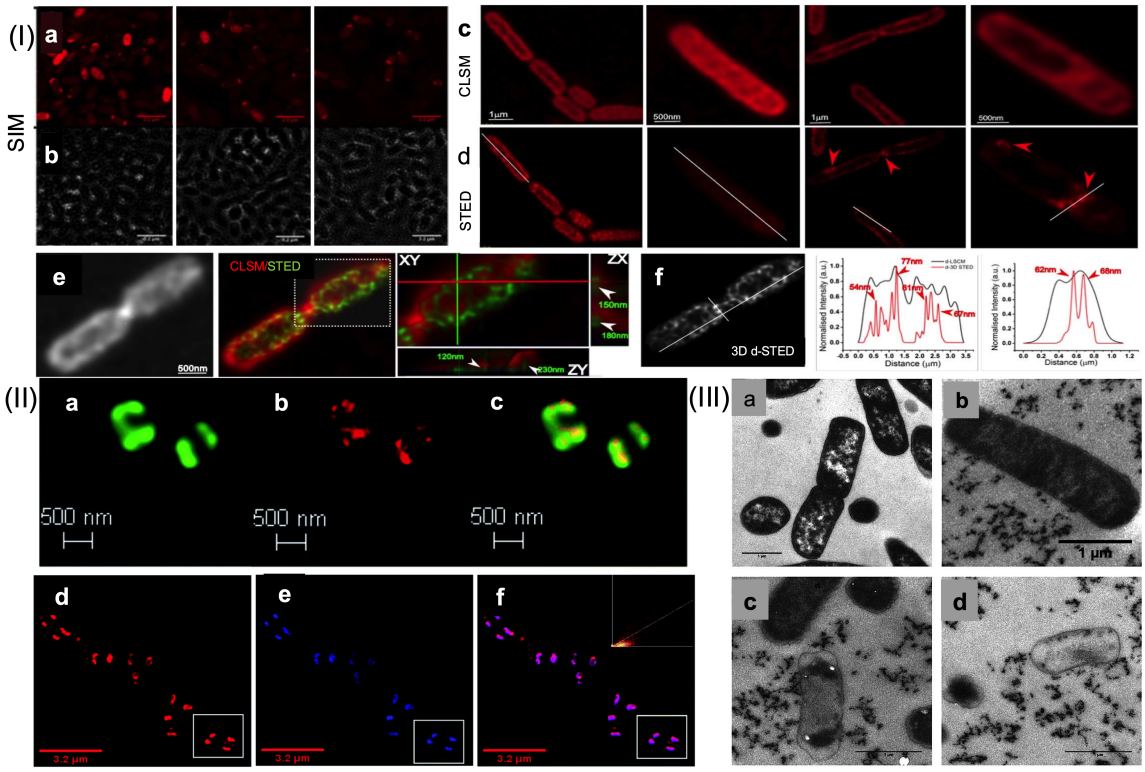

Figure 4|. **SRM imaging of bacteria using antimicrobial theragnostic complexes 4 and 5.** (I) SIM images to visualize the localization of **4** in E. coli EC958 cells at 5, 20, and 60 min: (a) Fixed cells are imaged using the luminescence of **4** (λ_{ex} = 450 nm/ A568 filter) and (b) phase contrast images; (c) CLSM (λ_{ex} = 470 nm) and STED images (775 nm depletion laser, and a 780 nm vortex phase plate) at 5, 20, 60, and 120 min. (e & f): Representative images showing section planes of full-volume deconvoluted d-LSCM and d-3D STED of E. coli EC958 cells: Normalized emission intensity profile (Black line: d-CLSM and Red line: d-3D STED) of the solid white lines drawn on top of selected region of cells are plotted. (II) Visualization of localization of **5** in *S. aureus* SH1000 cells using (a) d-CLSM (green), (b) STED nanoscopy (red) and (c) overlay image at 120 min incubation; (d-f) SIM images (Co-staining using DAPI (300 nm)) using **5** at 60 min incubation: (d) **5**; (e) DAPI and (f), overlay of **5** and DAPI with colocalization scatter plot. [λ_{ex} = 488 nm using A568 filter/ For DAPI λ_{ex} = 405 nm using the DAPI filter]. (iii) TEM images: Localization of **5** in *E. coli* EC958 cells following treatment with MIC concentrations of 6 (a) 0 min, (b) 10 min (c), 60 min (d) 120 min after exposure. Cell leakage/debris is revealed in b and c, although the images in c and c reveal membranes that are still intact. [Bar = 1 µm in all TEM images]. Reprinted with permission from ref. 74 and 75. Parts (I) adapted with permission from ref. 74, American Chemical Society. Part (II) and (III) reprinted with permission from ref. 75, Royal Society of Chemistry.

The Thomas group went on to examine the bactericidal properties of complexes related to **3** and identified promising leads that display broad-spectrum activity with low minimum inhibitory concentration, MICs, even in multidrug-resistant, MDR, strains. In this work, the multimodal imaging capabilities of the newly identified complexes facilitated investigations into their mechanism of action. For example, through SRM studies the activity of complex **4** was attributed

to its ability to disrupt the cell walls and outer membranes of Gram-positive and Gram-negative bacteria. 3-D STED images of the pathogenic EC958 *E coli* MDR strain treated with **4** showed that that the cationic compound rapidly localizes on the negatively charged bacterial outer membrane, followed by internalization. TEM images confirmed the compound-induced cell lysis in the same time window (<1 hour) - Fig 4. [74]

Subsequent studies revealed that complex **5**, the mononuclear analogue of **4**, is also a broad-spectrum antimicrobial reagent. MIC values for **5** are comparable to ampicillin and oxacillin and, like **4**, it also maintains its activity in pathogenic multi- and pan-drug resistant strains. SRM studies revealed that, unlike its dinuclear analogue, complex **5** is cell permeant and also has a different mode of action. [75] SIM and STED studies, used to identify its intracellular targets within *EC958* and *S aureus* cells, showed that **5** adopted a distinctive localization pattern quite different to that for **4**, which is characteristic of bacterial DNA staining; while TEM images confirmed that bacterial membranes were still largely intact after treatment and cell death - Fig 4.

Probes containing other second- and third-row d^6 transition metal centers

The cell uptake and SRM imaging capabilities of dinuclear Ru/Re complexes have also been reported by the Thomas group and collaborators. Complexes **6** and **7** incorporate two potential DNA intercalating moieties linked by different linking ligand "tethers". Although these systems were found to bind to DNA with comparable affinities, [76-78] steady-state and time correlated single photon counting (TCSPC) studies revealed the presence of the amine functionalities in the linker of **7** had a significant influence on the intracellular localizations and imaging properties of the complexes – Fig 5.

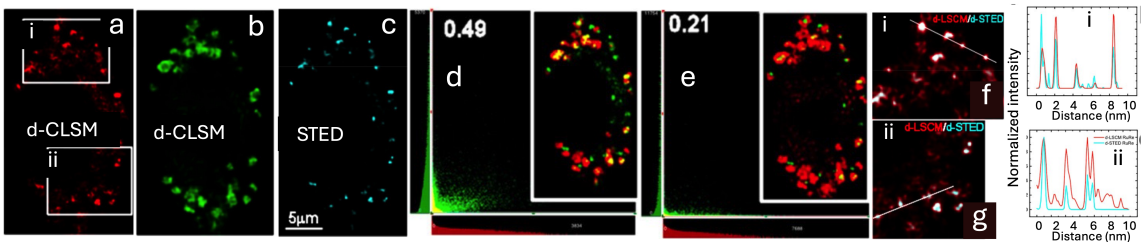

Figure 5| **Live MCF-7 cell uptake of Ru/Re complex 7; comparison of deconvoluted-CLSM images and deconvoluted STED (d-STED) microscopic images**. CLSM images of mitochondrial staining with **7** is shown in red (a), with Mitotracker in Green (b), and STEM image with in cyan (c). White squared insets (i) and (i) in (a), are magnified in (f) and (g), respectively; d-CLSM in red and-STED in cyan are shown. (d) and (e) show 2D scatter plot and surface map to reveal that the colocalized objects in yellow. Normalized intensity line profiles of the white lines in (f for region i) and (g for region ii) are also shown. Reprinted with permission from ref. 76, American Chemical Society.

Importantly, complex **7** showed concentration-dependent localization and photophysical properties that were suited to SIM and STED nanoscopies, which enabled tracking the dynamics of the subcellular localization within live cells at sub-diffraction limits. It is well-established that light-switch complexes show "switch-on" emission responses in lipophilic environments, including lipid-rich regions.[79,80] The fact that emission for complex **7** is seen from lysosomes and mitochondria suggests the complex localizes in such environments.

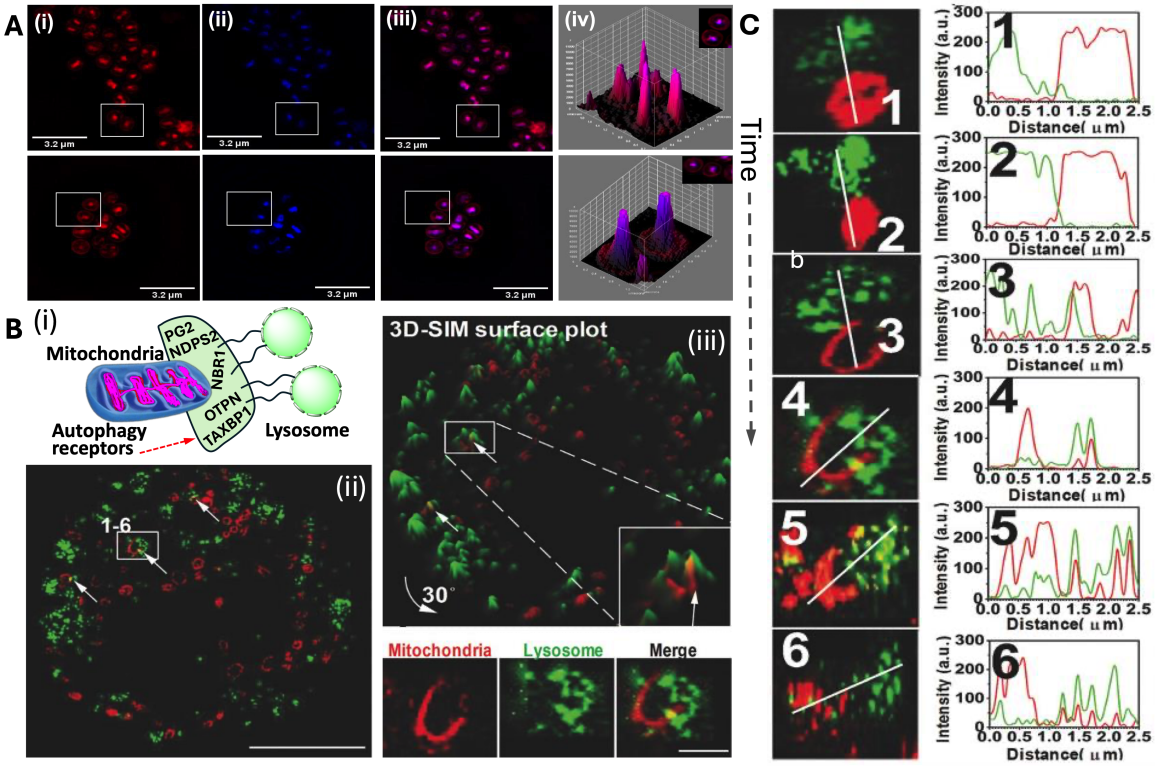

Figure 6| **Examples of the use of Os^{II} and Ir^{III} complexes as super-resolutions live cell probes in both prokaryotes and eukaryotes**. **A.** SIM images to real the uptake of Os complexes by *S. aureus* (MRSA strain) cells. 3D Z-stack projection, SIM colocalisation study using *S. aureus* MRSA after 1 hour incubation of cells with MIC concentrations of *fac*-**10** (top) and *mer*-**10** (bottom). (i) Image obtained on excitation of **10** (ii) Images obtained by simultaneous staining with DAPI. (iii) Overlay of both channels. (iv) 3D surface plots for the selected cells shown in the corresponding white boxes of the colocalization images, showing emission intensity for **10** and DAPI. **B.** (i) cartoon representation for mitochondria–lysosome (MLC) contact, (ii) and (iii): Images for tracking MLC contact in live Penta knockout HeLa cells using complex **11**. Left: cells treated with 10×10^{-6} M carbonyl cyanide *m*-chlorophenyl hydrazone (CCCP) for 12 h [Scale bars = 10.0 µm]. Insert: White rectangle to show MLC, (presented in **C**) [Scale bars = 1.00 µm]. Right, top: 3D SIM surface plot after 30° rotation with white arrows to identify MLC events. Right, bottom: expanded images to reveal a representative MLC event. **C**. 1-6: Time evolution of one MLC in a living cell; white solid lines indicate fluorescence intensity shown to the right. [Scale bars: (a) 10.0 µm, (b) 1.0 µm]. Reprinted with permission from ref. 82 and 85. Parts (A) adapted with permission from ref. 82, Royal Society of Chemistry. Part (B) and (C) are reprinted with permission from ref. 85, Wiley.

Analogous Os(II)-tris2,2'-bipyridyl derivatives (**8** – **10**) also possess exceptional stability towards photobleaching, high luminescence quantum yield, long-lived luminescence, and large Stokes shift, which minimize background noise. For example, an Os^{II} complex closely related to **3** was found to have very similar multimodal imaging properties. However, thanks to a red shift in emission (λ_{em} >750 nm), this system functions as a near-infrared STED probe.[81] The mechanism of action of potential therapeutics based on Os(II) centres has also been explored by SIM. The diastereomers (mer- and fac- forms) of complexes **8** – **10** were synthesized and isolated and their efficacies as antimicrobials were investigated.[82] These six complexes were found to be active against Gram-positive bacteria with mer-**10** being the most active against pathogenic strains at

activities comparable to conventional antibiotics. SIM studies with this complex, which displays red emission, showed cellular uptake within MRSA cells (Fig. 6A) and revealed clear binding to bacterial DNA (Pearson's coefficient: ~ 0.95 with DAPI).

The in-cell properties of several cyclcometalated Ir^{III} complexes have been investigated. [83,84] In 2018, the Chao group used complex **11** to track mitochondria and their dynamics in live cells through SIM at ~80 nm resolutions (Fig. 6B). [85] As the probe provided detailed images of mitochondrial ultrastructures such as christae, the authors concluded it specifically binds to mitochondrial membranes. The probe could also be used to temporally track mitochondrial fission and fusion dynamics.[86] In combination with the commercial probe, LysoTracker Green, complex **11** was also used to reveal hitherto unseen details of close mitochondria-lysosome membrane contacts and observe the organelles fusion after mitochondrial-damage-induced mitophagy (Fig. 6B and C). [85]

The route toward super-resolution CLEM

Transition complexes of d^6-metal centers have also found a role as probes for combined super-resolution imaging modalities. An area with particular potential is correlative light electron microscopy, CLEM, [87,88] which offers the possibility of combining both imaging selectivity and nanometer resolution to provide structural and dynamic details of cellular ultra-structures. While the use of Ir^{III}-complexes as multimodal SIM/TEM probes had already been demonstrated,[89] the first successful demonstration of true super-resolution CLEM with a metal complex appeared in a report from the Zhang, Tian, and Battaglia groups, who reported on a cyclometalated Ir^{III}-complex **12** capable of binding to tubulin at vinblastine biding sites, [90] a molecule with which it bears some similarities. Complex **12** displayed low toxicity toward both cancer-derived (A549, HeLa, MCF-7, HepG2, and HEK), and primary cell lines (HDF and HELF) and shows a bright red "switch-on" luminescence which is specifically induced by binding to tubulin - Fig. 7A. This observation was confirmed through co-localization with an α-tubulin antibody and microtubules in fixed cells. This approach provided a fundamental tool to monitor microtubule dynamics in live cells during mitosis and image microtubule-rich hippocampal tissue. By combining this capability with the contrast enhancement **13** provides in TEM, CLEM imaging was accomplished, Fig 7B, so that *individual* intracellular microtubules could be identified at up to sub-nanometre resolutions.

In a subsequent study, an iridium(III) complex that can image a second cytoskeletal element was reported.[91] Complex **13** is non-emissive in solution; however, when its weakly coordinated water molecules are displaced by direct coordination to His40 amino acid residues on actin protein fibers, the emission is switched on – Fig 7C. This effect is specific to actin as minimal emission enhancement is observed with other proteins and amino acids. By exploiting this effect, STED images of actin fibers in live HFL1 fibroblasts could be generated. Through correlating the emission of **13** in ultrathin cell sections with corresponding scanning-TEM images individual 8 nm diameter actin filaments could be resolved – Fig 7D.

CLEM imaging of intracellular DNA structure has also been accomplished using "DNA light-switch" complexes **14** and **15**. As mentioned above, such complexes are non-emissive in aqueous solution and only display their characteristic M→dppz-based emission when they intercalate into DNA.

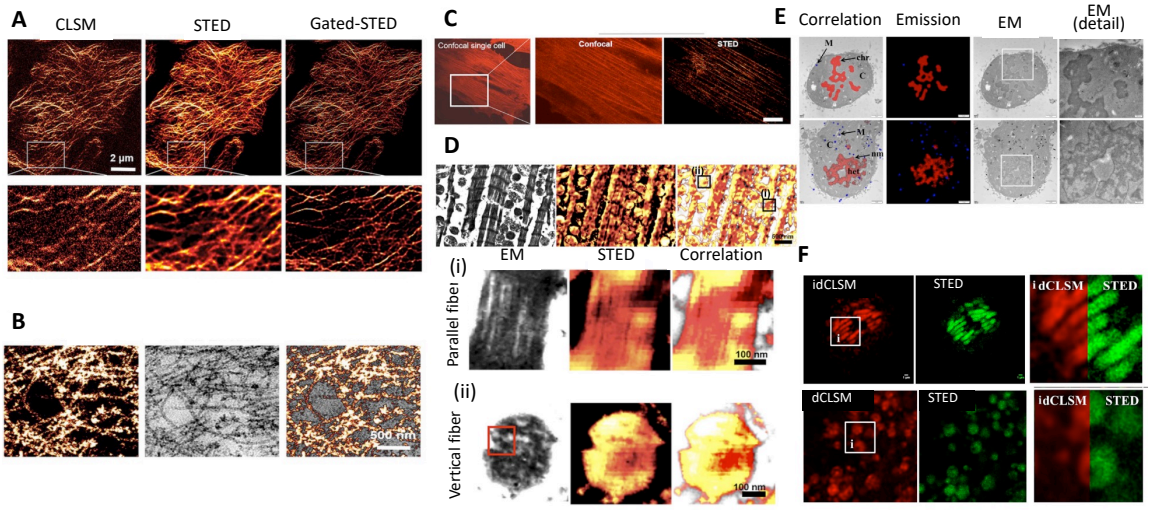

Figure 7| **Correlative light electron microscopy, CLEM, can be combined with SRM when using selected metal complexes**. **A**. HepG2 cell fixed and stained with 5× 10^{-6} M of **12;** microtubule images by confocal, STED (full power) and time-gated STED (15 ns) microscopy. **B**. Fluorescence imaging (left), scanning–transmission electron microscopy (center) and CLEM (right) images of microtubules labelled with **12** in HepG2 cells. The images obtained using light and EM microscopy were taken from the same site. **C**. Confocal and STED imaging of live HFL1 cells labelled with 5 μM **13** for an incubation period of 60 min Scale bar = 2 μm. **D**. Fibril structure of mouse heart tissue treated with **13** revealed by scanning-transmission electron microscopy (left-hand side), STED (center) and Correlation Light-Electron Microscopy (CLEM) (right-hand side). (i) and (ii) show zoomed-in views of parallel (i) and vertical (ii) actin filaments via CLEM. **E**. CLEM images show mitotic cells stained by **14** visualizing chromosome aggregation and decondensation during mitosis. Cells stained with **14** after fixation. **F**. Top: Deconvoluted CLSM (left) and STED images (right) of chromosomes stained by **15** during metaphase. Right: enhanced resolution by STED can be observed in the comparison of dCLSM / STED images in enlarged box (i). Bottom: corresponding data after protocol for mitochondria. Reprinted with permission from ref. 90, 91, 92 and 93. Parts (A) and (B) adapted with permission from ref. 90, Wiley. Part (C) and (D) reprinted with permission from ref. 91, Elsevier. Part (E) reprinted with permission from ref. 92, American Chemical Society. Part (F) reprinted with permission from ref. 93, Oxford University Press.

Although these complexes are not usually cell-permeant, the Zhu group have reported that if ion paired with 2,3,4,5-tetrachlorophenolate, TeCP, counter-anions they can be delivered into live cells and their imaging capability is dependent on the enantiomer employed. The osmium(II) complex 1**4** has a characteristic deep red emission (λ_{em} = 750 nm) when bound to DNA and it was reported that when delivered through this method into HeLa cells Δ-**14** displayed much higher nuclear emission than Λ-**14** even though both enantiomers are taken up at comparable concentrations. This effect resulted in well-defined SIM images of nuclear DNA. Furthermore, the complex still displayed pronounced luminescence after cells were fixed, treated with OsO_4 and processed for TEM imaging, thus providing the opportunity to produce SR-optical/electron microscopy CLEM images of nuclear DNA and even chromosomal aggregation in mitosis – Fig 7E.[92] A recent report from the same researchers on the related ruthenium complex **15** has described a method to selectively image nuclear *and* mitochondrial DNA.

As might be expected, the authors report that complex **15** could be used as a STED probe for nuclear DNA when delivered through ion-pairing with TeCP. However, if HeLa cells treated this way were then washed with fresh buffer and incubated for a further 3 hours, the complex was found to shift its localization to mitochondria. Colocalization studies with probes such as picogreen offered evidence that the complex specifically binds to mitochondrial DNA, mtDNA. Again, it was found that Δ-**15** displayed brighter emission from nuclei or mitochondria than Λ-**15**. So, using this protocol, SR-images of both nuclear and mt-DNA were obtained Fig 7F. [93]

Platinum(II) probes

Apart from d^6-octahedral complexes, another metal center that has attracted attention for SR applications is the square planar Pt(II) d^8 electronic configuration. Normally, bi- and tri-dentate Pt(II) complexes with the general formula $[Pt(N\wedge N)_2Cl_2$ or $[Pt(N\wedge N\wedge N)Cl]^+$ (N∧N∧N: 2,2':6',2''-terpyridine or its derivatives) are non-emissive or possess negligible luminescence quantum yield at room temperature due to an efficient non-radiative decay involving low-lying MC (d–d) excited states. [94,95] However, the replacement of Cl^- with a strong-field ligand raises the energy of the deactivating *d–d* states to facilitate room temperature luminescence. [96,97] Importantly, the Pt(II)-center favors mixing of the singlet and triplet manifolds due to effective spin-orbit coupling and efficiently populates the first excited triplet state (T_1), [95,97] which leads to emission lifetimes in the range of hundreds of nanoseconds to tens of microseconds.

Using this effect, the Yam research group reported on a binuclear platinum complex **16** with a large Stokes shift (λ_{ex} = 405 nm, λ_{em} = 530 nm and 700 nm / τ_{avg} = 10.8 μs; λ_{ex} = 488 nm, λ_{em} = 700/ τ_{avg} = 0.16 μs) (Fig 7).[98] Complex **16** was found to be an attractive dye for SIM as it displays negligible photobleaching and could specifically label autolysosome in live HeLa cells Fig 8A. These images revealed that upon continuous light stimulation, the luminescence intensity of autolysosomes decreased gradually, while that of the nucleus increased gradually, indicating that **16** escapes from autolysosomes to the nucleus (Fig. 8B and C). As autophagy plays a very significant role in tumor genesis, the real-time tracking of autolysosomes by this probe may have a role in diagnosis.

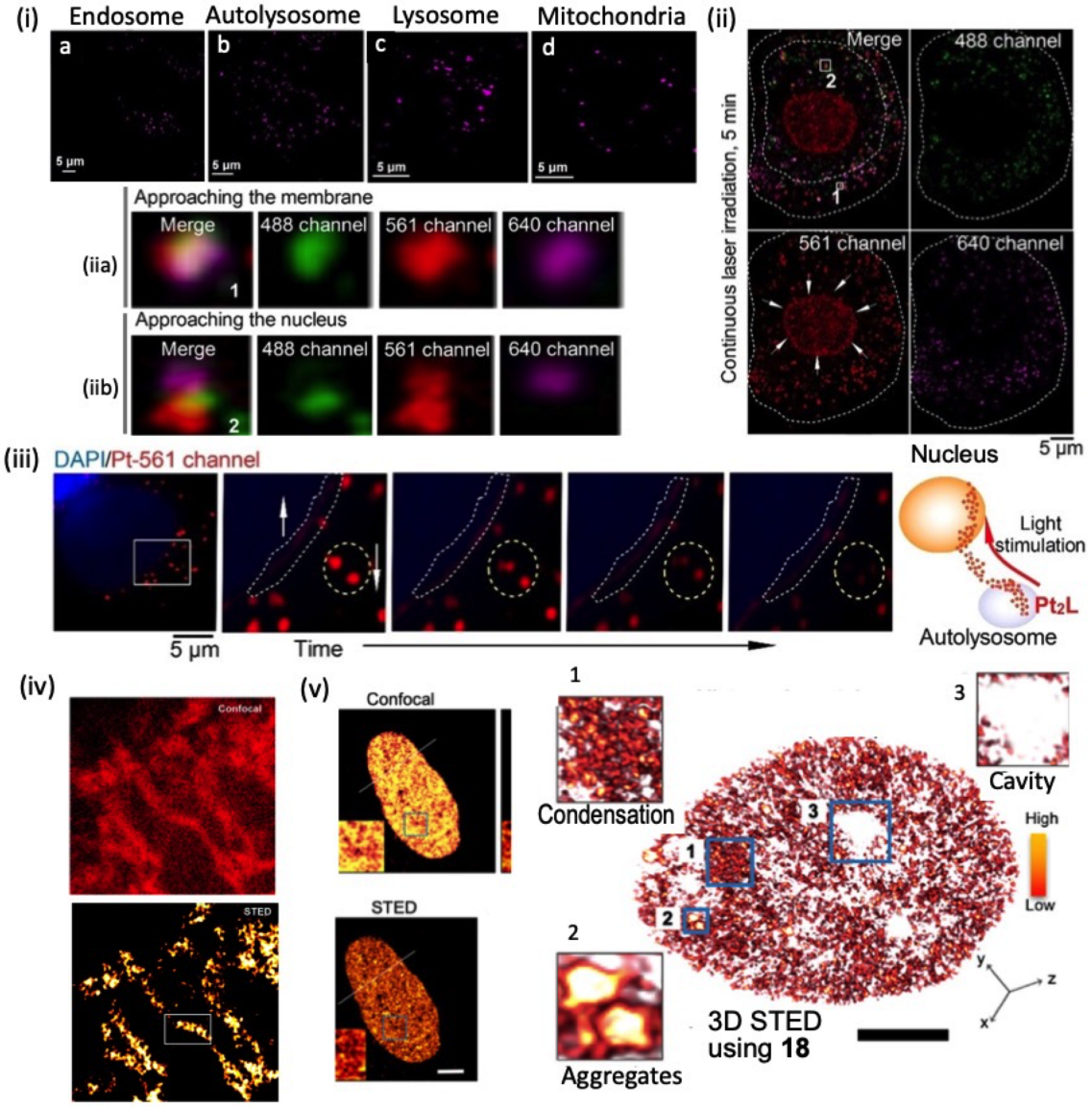

Figure 8| **Specifically imaging cellular processes and sub-organelle structures with late-transition or post transition metal complexes**. I. SIM images for colocalization of **16** within (a) endosome, (b) autolysosome, (c) lysosome and (d) mitochondria. Images were observed under SIM 640 and 561 or 488 nm channels, (Pearson's correlation coefficient, PCC). II. Co-localization of **16** in different SIM channels (merged, 640 and 561 or 488 nm channel) following laser irradiation for 5 min; (IIa) expansion of white rectangle 1 showing co-localization of **16** in the membrane and (IIb) Expansion of white rectangle 2 showing co-localization of **16** with the nucleus. III. The dynamics process of photoactivated **16** escaping from the autolysosomes to the nucleus, with the luminescence intensity gradually decreasing in autolysosomes and increasing in the nucleus. IV. The CLSM and STED images (λ_{ex} = 405 nm, λ_{em} = 595 nm) of live HepG2 cells stained with **17**. V. Left: 3D-STED images of SiR-DNA staining (λ_{ex} = 670 nm and λ_{em}=700 nm) of live HepG2 cells treated with **18**. Right: ITSA1 (histone deacetylase activator) treated cells (to activate histone acetylation), incubated with **18**, imaged under STED to construct the 3D micrograph: note that the selected ROI highlighted (1-3) represent; histone condensation, aggregates, and cavity regions

(Scale bar = 2 µm). Reprinted with permission from ref. 98, 99 and 101. Parts (I) - (III) adapted with permission from ref. 98, Wiley. Part (IV) reprinted with permission from ref. 99, Royal Society of Chemistry. Part (V) reprinted with permission from ref. 101, American Chemical Society.

Box 3 | The potential of first-row transition metal complexes

As the above examples illustrate, over the last decade, precious metal complexes have proven to possess great potential as probes for super-resolution microscopy. However, many of these metals have low abundance and are correspondingly expensive. Although this may not be a limiting factor in such specialized applications, probes constructed from more readily available, earth-abundant metals would offer an attractive alternative and recently the possibilities of such systems have begun to be investigated.

First-row transition metal ions with d^6 configuration (eg; Fe^{2+}, Co^{3+}) effectively populate ^{1}MLCT electronically excited on photoexcitation at the respective absorption maximum. However, for first-row d^6 transition metal complexes, the crystal field splitting (Δ) is smaller than second and third-row transition metal ions, which is attributed to a lower energy for the ^{1}MC and ^{3}MC states than ^{1}MLCT and T^1 states. This accounts for a faster deactivation of the excited states. Recent reports suggest that with appropriate chelating ligand design, it is possible to develop metastable first-row transition metal ion complexes (lifetime ≤ 10 ns). While the photochemistry of metal complexes having d^7 (Co^{2+}, Ni^{3+}) and d^8 (Ni^{3+}) electronic configurations is less rich than d^6 in terms of photo- and redox-stabilities, photosensitizers derived from metal ions with $3d^{10}$ (Cu^+, Zn^{2+}) electronic configuration do show interesting properties. A filled electronic *d*-shell eliminates the MC states and allows relatively more stable ^{3}MLCT states to dominate photophysical properties. Hence the emergence of the use of Zn^{2+} complexes as imaging reagents.

Multifunctional super-resolution probes based on first-row transition metals

Tian, *et al*. have investigated the SR imaging capabilities of several first-row transition metal complexes. They specifically targeted mitochondria using a Zn(II)-based complex, **17**, that incorporated terpyridyl-based ligands connected to thiophene units to extend electronic delocalization. [99] The presence of an organic ligand with donor-π-acceptor interactions favoring a distinct push-pull electron effect accounts for its unique optical properties. [100] This complex, which displays red-emission assigned to a photostable MLCT excited state, was found to bind to mtDNA in cell-free conditions. It is taken up by live HepG2 cells and co-localizes with MitoTracker Deep-Red, confirming its mitochondrial localization. More detailed tests revealed that **17** binds to mtDNA and not mitochondrial membranes and live-cell STED produced detailed images of the folded crista structures within mitochondria -Fig 8D.

In a follow-up study, a STED probe for the imaging of histones and histone processing was developed. In this report, the same central $Zn^{II}(tpy)_2$ unit was appended with electron-rich azide moieties on the periphery of the tpy ligands, which provide a targeting moiety for the cationic charge of histones, to yield complex **18**.[101] In cell-free conditions, involving various possible substrates including amino acids and nucleic acids, it was found that binding to histones uniquely resulted in a large increase in its green emission, which also blue-shifted by 25 nm. As the complex showed low toxicity toward HepG2 cells, its potential for live-cell STED imaging was investigated.

Through CLSM imaging, it was found that the complex was cell-permeant and localized in the nucleus, while studies involving ribonucleases confirmed that its binding target within this location was neither DNA nor RNA. In-cell histone binding was confirmed by colocalization with a fluorescent anti-histone antibody. The researcher then went on to show that the increased resolution provided by STED, meant that **18** could be used in live cells to investigate and image morphology changes, such as condensation, induced by histone acetylation -Fig 8E and F.

Related terpyridyl ligands were also used in the construction of Mn^{II} complexes for multimodal SR images. The first study on such systems involved the identification of a complex that could be used for both STED and magnetic resonance imaging. This is an attractive proposition as, taken together, the two modalities offer a combination of imaging live cells at tens of nanometers resolution and the capability of visualizing tissue at depth. The extended tpy ligands of complexes **19** incorporate triphenylamine groups as electron donors and hydroxymethyl moieties to improve water solubility and its coordination with Mn^{II} provides a paramagnetic center for MRI.

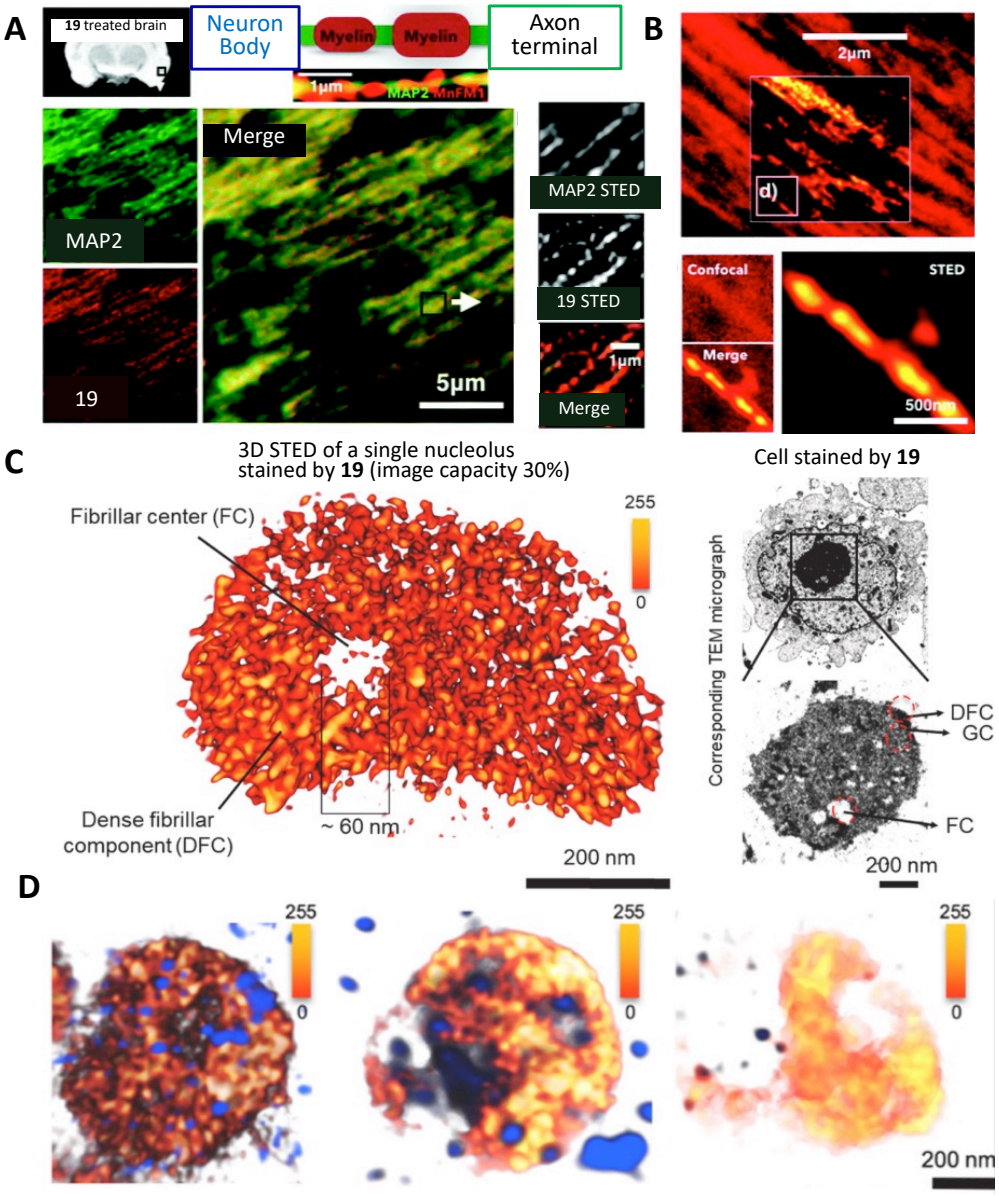

Figure 9| **Examples of using Mn^{II} complexes as multimodal SRM probes**. A. Top: MR micrographs of a mouse brain incubated with **19.** Bottom: (Left) CLSM colocalization staining of a brain slice with **19** and MAP2 antibody used to mark neurons; (Right) STED micrograph from a selected region showing myelin and axon structures. B. Top: CLSM and STED micrographs of the brain slice treated with **19** Bottom: a selected region (Box c in the upper image) showing a single myelin wrapping the axon fibre. C. Left: 3D-STED micrograph of the ultra-details of a single nucleolus stained with 10 μM complex, **20.** Right: TEM a micrograph of cells incubated with 20 μM of **20** and stained without osmium tetroxide clearly showed the structure of different regions of the nucleolus. D. Three-dimensional confocal laser scanning images of fixed HeLa cells incubated with 10 μM complex, **20** for 30 min and immunofluorescent label with a ribosome marker - monoclonal to RPS3, after 6 h of insulin treatment, 6 h of starvation treatment, and normal culture, respectively. Reprinted with permission from ref. 102 and 104. Parts (A) and (B) adapted with permission from ref. 102, Royal Society of Chemistry. Part (C) and (D) reprinted with permission from ref. 104, Elsevier.

The complex was found to internalize within HepG2 cells and its MLCT luminescence was compatible with both conventional and two-photon absorbance CLSM. Using these techniques, co-localization studies with commercial probes, as well as ICP-MS, revealed that the complex is distributed throughout the cytosolic region in the lipid-rich ER. The authors then went on to demonstrate the potential of **19** for multiscale imaging using *ex-vivo* tissue and whole organs.[102] For example, not only could an entire mouse brain be imaged at enhanced contrasts through MRI when treated with the complex, but -when sectioned into 20 μm slices- details of the myelin sheaths of individual neuronal axons could be obtained using the luminescent properties of **19** - Fig 9A and B.

Consequently, a recent report has extended this approach, demonstrating how a thermodynamically stable Mn(II)-complex of a salen-derivative incorporated within a porous SiO_2-nanoparticle decorated with folate moieties (Average diameter of 19.3 ± 2 nm) could be exploited for multimodal imaging, including magnetic resonance imaging.[103]

The nucleolus is the largest intranuclear organelle and is the ribosome factory of the cell, where ribosome components are processed and assembled. As highly proliferative cancer cells have an increased demand for protein synthesis, they frequently possess enlarged nucleoli. The nucleolus also has a role to play in a variety of processes ranging from stress sensing to telomere formation and, apart from carcinogenesis, nucleolar dysfunction is associated with a variety of other diseases including neurodegenerative disorders. Consequently, probes that could image the nucleolus and its dynamics at high resolutions would have relevance across a range of disciplines, from fundamental studies in cell biology to diagnostic devices.

The structure of **19** was adapted to yield a complex that could be used as an STED probe for nucleolar RNA. Highly charged complex, **20** incorporates a tpy ligand which in itself had previously been shown to target ribosomal RNA in live cells. Cell-free studies with a variety of biomolecules showed that the intensity of the emission from the complex is significantly enhanced and red-shifted only when binding to RNA. CLS-based colocalization experiments in live HeLa cells using small molecule probes and specific immunofluorescent proteins, as well as ribonuclease-based digests, confirmed that **20** localizes in and stains nucleolar RNA.[104] However, by exploiting the excellent STED capabilities of the complex, highly detailed images revealing individual compartments within the nucleolus were obtained -Fig 9C. In particular, dense and porous fibrillar structures were observed, which were interpreted as being the dense fibrillar component, DFC,

and fibrillar centres, FC. The FC mostly contains RNA polymerase I sub-units and pre-rRNA transcripts are found in the DFC, with actual transcription of rRNA largely occurring at the FC-DFC boundary. By also using an immunofluorescent labelling antibody for ribosomes themselves, [105] the authors went on to use STED to investigate cells where translation rates were modulated either by exposure to insulin or serum starvation. In these experiments distinctive changes in the number, size, and morphology of FCs as well as ribosome aggregation were observed and quantified – Fig 9D.

Conclusions and Outlook

In the last two decades, the number of techniques and possible applications of SRM have burgeoned. Optical nanoscopy at ~10 nm scales are now commonplace and, with the recent development of MINFLUX, spatial resolutions down to 1 nm, along with millisecond time resolutions, in live cells have been claimed.[106-109] However, all these new techniques are reliant on identifying dedicated probes with highly defined photophysical and biophysical properties.[110] In this context, the facile tunability of both the functional group chemistry and photo-excited states of metal complexes through designed synthesis offers great potential and new opportunities in developing targeted probes for specific SRM modalities. As illustrated by several examples discussed above, this is particularly true in terms of multimodal imaging and multiplex imaging. Also, designing dedicated correlative light and electron microscopy (CLEM) probes to enable researchers to directly correlate information obtained on a light and an electron microscope. The quest for multimodal probes that are both fluorescent and electron-dense not only will help researchers to label specific organelle/object(s) in a biological sample with improved resolution but also will enable them to precisely overlay electron and fluorescent images.

Although metal complexes are now being exploited in a wide range of SRM techniques, there are still lacunae to be filled. For example, there has been surprisingly little activity in exploring their use in stochastic imaging techniques, such as PALM and STORM.[111-115] Yet, as illustrated by the work reported by Tang, et al on Zn^{II}(salen) complexes STORM probes for mitochondria,[115] it is quite possible to produce metal complexes with innate high fluorescence ''off/on'' ratios and the organelle-specificity required for such entities. There is also a distinct need to focus on identifying organelle-specific transition metal complexes having distinctly different luminescence decay profile for simultaneous imaging of multiple organelle (multiplexing) to examine subtle interactions among immune cells, stroma, matrix, and malignant cells within the tumor microenvironment. Such information would have significant translational impact. However, challenges such as probe quenching, and non-uniform probe delivery can impact its effectiveness, particularly in thick or dense tissue samples. Despite these limitations, techniques, and probe design advancements continue to enhance its applicability for high-resolution tissue imaging.

References

1 Perego, E. *et al.* Single-photon microscopy to study biomolecular condensates. *Nature Communications* **14**, 8224, doi:10.1038/s41467-023-43969-7 (2023).

2 Strullu-Derrien, C. *et al.* A fungal plant pathogen discovered in the Devonian Rhynie Chert. *Nature Communications* **14**, 7932, doi:10.1038/s41467-023-43276-1 (2023).

3 Niu, X. *et al.* Corneal confocal microscopy may help to distinguish Multiple System Atrophy from Parkinson's disease. *npj Parkinson's Disease* **10**, 63, doi:10.1038/s41531-024-00680-8 (2024).

4 Li, W., Kaminski Schierle, G. S., Lei, B., Liu, Y. & Kaminski, C. F. Fluorescent Nanoparticles for Super-Resolution Imaging. *Chemical Reviews* **122**, 12495-12543, doi:10.1021/acs.chemrev.2c00050 (2022).

5 Pramanik, S. K. *et al.* Nanoparticles for super-resolution microscopy: intracellular delivery and molecular targeting. *Chemical Society Reviews* **51**, 9882-9916, doi:10.1039/D1CS00605C (2022).

6 Monge, R., Delord, T. & Meriles, C. A. Reversible optical data storage below the diffraction limit. *Nature Nanotechnology* **19**, 202-207, doi:10.1038/s41565-023-01542-9 (2024).

7 St. Croix, C. M., Shand, S. H. & Watkins, S. C. Confocal Microscopy: Comparisons, Applications, and Problems. *BioTechniques* **39**, S2-S5, doi:10.2144/000112089 (2005).

8 Yu, W., Rush, C., Tingey, M., Junod, S. & Yang, W. Application of Super-resolution SPEED Microscopy in the Study of Cellular Dynamics. *Chemical & Biomedical Imaging* **1**, 356-371, doi:10.1021/cbmi.3c00036 (2023).

9 Schermelleh, L. *et al.* Super-resolution microscopy demystified. *Nature Cell Biology* **21**, 72-84, doi:10.1038/s41556-018-0251-8 (2019).

10 Fu, P. *et al.* Super-resolution imaging of non-fluorescent molecules by photothermal relaxation localization microscopy. *Nature Photonics* **17**, 330-337, doi:10.1038/s41566-022-01143-3 (2023).

11 Kwon, J., Elgawish, M. S. & Shim, S.-H. Bleaching-Resistant Super-Resolution Fluorescence Microscopy. *Advanced Science* **9**, 2101817, doi:https://doi.org/10.1002/advs.202101817 (2022).

12 Zhuang, Y. & Shi, X. Expansion microscopy: A chemical approach for super-resolution microscopy. *Current Opinion in Structural Biology* **81**, 102614, doi:https://doi.org/10.1016/j.sbi.2023.102614 (2023).

13 Sednev, M. V., Belov, V. N. & Hell, S. W. Fluorescent dyes with large Stokes shifts for super-resolution optical microscopy of biological objects: a review. *Methods and Applications in Fluorescence* **3**, 042004, doi:10.1088/2050-6120/3/4/042004 (2015).

14 Gustafsson, M. G. L. Nonlinear structured-illumination microscopy: Wide-field fluorescence imaging with theoretically unlimited resolution. *Proceedings of the National Academy of Sciences* **102**, 13081-13086, doi:10.1073/pnas.0406877102 (2005).

15 Mortensen, K. I., Churchman, L. S., Spudich, J. A. & Flyvbjerg, H. Optimized localization analysis for single-molecule tracking and super-resolution microscopy. *Nature Methods* **7**, 377-381, doi:10.1038/nmeth.1447 (2010).

16 Thompson, R. E., Larson, D. R. & Webb, W. W. Precise Nanometer Localization Analysis for Individual Fluorescent Probes. *Biophysical Journal* **82**, 2775-2783, doi:https://doi.org/10.1016/S0006-3495(02)75618-X (2002).

17 Jiang, G. *et al.* A synergistic strategy to develop photostable and bright dyes with long Stokes shift for nanoscopy. *Nature Communications* **13**, 2264, doi:10.1038/s41467-022-29547-3 (2022).

18 Liu, S. *et al.* Super-resolved snapshot hyperspectral imaging of solid-state quantum emitters for high-throughput integrated quantum technologies. *Nature Photonics*, doi:10.1038/s41566-024-01449-4 (2024).

19 Möckl, L. & Moerner, W. E. Super-resolution Microscopy with Single Molecules in Biology and Beyond–Essentials, Current Trends, and Future Challenges. *Journal of the American Chemical Society* **142**, 17828-17844, doi:10.1021/jacs.0c08178 (2020).

20 Tholen, M. M. E., Tas, R. P., Wang, Y. & Albertazzi, L. Beyond DNA: new probes for PAINT super-resolution microscopy. *Chemical Communications* **59**, 8332-8342, doi:10.1039/D3CC00757J (2023).

21 Sahl, S. J., Hell, S. W. & Jakobs, S. Fluorescence nanoscopy in cell biology. *Nature Reviews Molecular Cell Biology* **18**, 685-701, doi:10.1038/nrm.2017.71 (2017).
22 Xiao, J. & Dufrêne, Y. F. Optical and force nanoscopy in microbiology. *Nature Microbiology* **1**, 16186, doi:10.1038/nmicrobiol.2016.186 (2016).
23 Nicovich, P. R., Owen, D. M. & Gaus, K. Turning single-molecule localization microscopy into a quantitative bioanalytical tool. *Nature Protocols* **12**, 453-460, doi:10.1038/nprot.2016.166 (2017).
24 Egner, A. & Hell, S. W. Fluorescence microscopy with super-resolved optical sections. *Trends in Cell Biology* **15**, 207-215, doi:https://doi.org/10.1016/j.tcb.2005.02.003 (2005).
25 Dedecker, P., Flors, C., Hotta, J.-i., Uji-i, H. & Hofkens, J. 3D Nanoscopy: Bringing Biological Nanostructures into Sharp Focus. *Angewandte Chemie International Edition* **46**, 8330-8332, doi:https://doi.org/10.1002/anie.200703314 (2007).
26 Wu, D. *et al.* The blood–brain barrier: structure, regulation, and drug delivery. *Signal Transduction and Targeted Therapy* **8**, 217, doi:10.1038/s41392-023-01481-w (2023).
27 Dhiman, S. *et al.* Can super-resolution microscopy become a standard characterization technique for materials chemistry? *Chemical Science* **13**, 2152-2166, doi:10.1039/D1SC05506B (2022).
28 Bond, C., Santiago-Ruiz, A. N., Tang, Q. & Lakadamyali, M. Technological advances in super-resolution microscopy to study cellular processes. *Molecular Cell* **82**, 315-332, doi:https://doi.org/10.1016/j.molcel.2021.12.022 (2022).
29 Bon, P. & Cognet, L. On Some Current Challenges in High-Resolution Optical Bioimaging. *ACS Photonics* **9**, 2538-2546, doi:10.1021/acsphotonics.2c00606 (2022).
30 Zwettler, F. U. *et al.* Molecular resolution imaging by post-labeling expansion single-molecule localization microscopy (Ex-SMLM). *Nature Communications* **11**, 3388, doi:10.1038/s41467-020-17086-8 (2020).
31 Behzadi, S. *et al.* Cellular uptake of nanoparticles: journey inside the cell. *Chemical Society Reviews* **46**, 4218-4244, doi:10.1039/C6CS00636A (2017).
32 Liu, X., Testa, B. & Fahr, A. Lipophilicity and its relationship with passive drug permeation. *Pharmaceutical research* **28**, 962-977, doi:10.1007/s11095-010-0303-7 (2011).
33 Augustine, R. *et al.* Cellular uptake and retention of nanoparticles: Insights on particle properties and interaction with cellular components. *Materials Today Communications* **25**, 101692, doi:https://doi.org/10.1016/j.mtcomm.2020.101692 (2020).
34 Jin, Y., Tan, Y., Wu, J. & Ren, Z. Lipid droplets: a cellular organelle vital in cancer cells. *Cell Death Discovery* **9**, 254, doi:10.1038/s41420-023-01493-z (2023).
35 Dankovich, T. M. & Rizzoli, S. O. Challenges facing quantitative large-scale optical super-resolution, and some simple solutions. *iScience* **24**, 102134, doi:https://doi.org/10.1016/j.isci.2021.102134 (2021).
36 Jin, D. *et al.* Nanoparticles for super-resolution microscopy and single-molecule tracking. *Nature Methods* **15**, 415-423, doi:10.1038/s41592-018-0012-4 (2018).
37 Laissue, P. P., Alghamdi, R. A., Tomancak, P., Reynaud, E. G. & Shroff, H. Assessing phototoxicity in live fluorescence imaging. *Nature Methods* **14**, 657-661, doi:10.1038/nmeth.4344 (2017).
38 Kiepas, A., Voorand, E., Mubaid, F., Siegel, P. M. & Brown, C. M. Optimizing live-cell fluorescence imaging conditions to minimize phototoxicity. *Journal of cell science* **133**, doi:10.1242/jcs.242834 (2020).
39 Kasprzycka, W., Szumigraj, W., Wachulak, P. & Trafny, E. A. New approaches for low phototoxicity imaging of living cells and tissues. *BioEssays* **46**, 2300122, doi:https://doi.org/10.1002/bies.202300122 (2024).

40 Foote, C. S. DEFINITION OF TYPE I and TYPE II PHOTOSENSITIZED OXIDATION. *Photochemistry and Photobiology* **54**, 659-659, doi:https://doi.org/10.1111/j.1751-1097.1991.tb02071.x (1991).

41 Garcia-Diaz, M., Huang, Y.-Y. & Hamblin, M. R. Use of fluorescent probes for ROS to tease apart Type I and Type II photochemical pathways in photodynamic therapy. *Methods* **109**, 158-166, doi:https://doi.org/10.1016/j.ymeth.2016.06.025 (2016).

42 Juarranz, A., Jaén, P., Sanz-Rodríguez, F., Cuevas, J. & González, S. Photodynamic therapy of cancer. Basic principles and applications. *Clinical & translational oncology : official publication of the Federation of Spanish Oncology Societies and of the National Cancer Institute of Mexico* **10**, 148-154, doi:10.1007/s12094-008-0172-2 (2008).

43 Celli, J. P. *et al.* Imaging and Photodynamic Therapy: Mechanisms, Monitoring, and Optimization. *Chemical Reviews* **110**, 2795-2838, doi:10.1021/cr900300p (2010).

44 Icha, J., Weber, M., Waters, J. C. & Norden, C. Phototoxicity in live fluorescence microscopy, and how to avoid it. *Bioessays* **39**, doi:10.1002/bies.201700003 (2017).

45 Glazer, E. C., Magde, D. & Tor, Y. Ruthenium Complexes That Break the Rules: Structural Features Controlling Dual Emission. *Journal of the American Chemical Society* **129**, 8544-8551, doi:10.1021/ja071124f (2007).

46 Gill, M. R. & Thomas, J. A. Ruthenium(ii) polypyridyl complexes and DNA—from structural probes to cellular imaging and therapeutics. *Chemical Society Reviews* **41**, 3179-3192, doi:10.1039/C2CS15299A (2012).

47 G, U. R. *et al.* A novel fluorescence probe for estimation of cysteine/histidine in human blood plasma and recognition of endogenous cysteine in live Hct116 cells. *Chemical Communications* **50**, 9899-9902, doi:10.1039/C4CC04214J (2014).

48 Shum, J., Leung, P. K.-K. & Lo, K. K.-W. Luminescent Ruthenium(II) Polypyridine Complexes for a Wide Variety of Biomolecular and Cellular Applications. *Inorganic Chemistry* **58**, 2231-2247, doi:10.1021/acs.inorgchem.8b02979 (2019).

49 Conti, L., Macedi, E., Giorgi, C., Valtancoli, B. & Fusi, V. Combination of light and Ru(II) polypyridyl complexes: Recent advances in the development of new anticancer drugs. *Coordination Chemistry Reviews* **469**, 214656, doi:https://doi.org/10.1016/j.ccr.2022.214656 (2022).

50 Jing, S. *et al.* Recent Advances in Organometallic NIR Iridium(III) Complexes for Detection and Therapy. *Molecules (Basel, Switzerland)* **29**, doi:10.3390/molecules29010256 (2024).

51 Zanoni, K. P. S. *et al.* Blue-Green Iridium(III) Emitter and Comprehensive Photophysical Elucidation of Heteroleptic Cyclometalated Iridium(III) Complexes. *Inorganic Chemistry* **53**, 4089-4099, doi:10.1021/ic500070s (2014).

52 Ghosh, H. N. & Das, A. in *Advances in Inorganic Chemistry* Vol. 81 (eds Debabrata Chatterjee & Rudi van Eldik) 305-343 (Academic Press, 2023).

53 Puckett, C. A. & Barton, J. K. Methods to Explore Cellular Uptake of Ruthenium Complexes. *Journal of the American Chemical Society* **129**, 46-47, doi:10.1021/ja0677564 (2007).

54 Notaro, A. *et al.* Ruthenium(II) Complex Containing a Redox-Active Semiquinonate Ligand as a Potential Chemotherapeutic Agent: From Synthesis to In Vivo Studies. *Journal of Medicinal Chemistry* **63**, 5568-5584, doi:10.1021/acs.jmedchem.0c00431 (2020).

55 Lee, H. & Dutta, P. K. Charge Transport through a Novel Zeolite Y Membrane by a Self-Exchange Process. *The Journal of Physical Chemistry B* **106**, 11898-11904, doi:10.1021/jp0208539 (2002).

56 Gonzalez-Vazquez, J. P., Burn, P. L. & Powell, B. J. Interplay of Zero-Field Splitting and Excited State Geometry Relaxation in fac-Ir(ppy)3. *Inorganic Chemistry* **54**, 10457-10461, doi:10.1021/acs.inorgchem.5b01918 (2015).

57 Pramanik, S. K. & Das, A. Fluorescent probes for imaging bioactive species in subcellular organelles. *Chemical Communications* **57**, 12058-12073, doi:10.1039/D1CC04273D (2021).
58 Singh, H., Tiwari, K., Tiwari, R., Pramanik, S. K. & Das, A. Small Molecule as Fluorescent Probes for Monitoring Intracellular Enzymatic Transformations. *Chemical Reviews* **119**, 11718-11760, doi:10.1021/acs.chemrev.9b00379 (2019).
59 Berezin, M. Y. & Achilefu, S. Fluorescence Lifetime Measurements and Biological Imaging. *Chemical Reviews* **110**, 2641-2684, doi:10.1021/cr900343z (2010).
60 Datta, R., Gillette, A., Stefely, M. & Skala, M. Recent innovations in fluorescence lifetime imaging microscopy for biology and medicine. *Journal of Biomedical Optics* **26**, 070603 (2021).
61 Ma, Y., Lee, Y., Best-Popescu, C. & Gao, L. High-speed compressed-sensing fluorescence lifetime imaging microscopy of live cells. *Proceedings of the National Academy of Sciences* **118**, e2004176118, doi:10.1073/pnas.2004176118 (2021).
62 BECKER, W. Fluorescence lifetime imaging – techniques and applications. *Journal of Microscopy* **247**, 119-136, doi:https://doi.org/10.1111/j.1365-2818.2012.03618.x (2012).
63 Schwehr, B. J., Hartnell, D., Massi, M. & Hackett, M. J. Luminescent Metal Complexes as Emerging Tools for Lipid Imaging. *Topics in Current Chemistry* **380**, 46, doi:10.1007/s41061-022-00400-x (2022).
64 Hell, S. W. & Wichmann, J. Breaking the diffraction resolution limit by stimulated emission: stimulated-emission-depletion fluorescence microscopy. *Opt. Lett.* **19**, 780-782, doi:10.1364/OL.19.000780 (1994).
65 Hofmann, M., Eggeling, C., Jakobs, S. & Hell, S. W. Breaking the diffraction barrier in fluorescence microscopy at low light intensities by using reversibly photoswitchable proteins. *Proceedings of the National Academy of Sciences* **102**, 17565-17569, doi:10.1073/pnas.0506010102 (2005).
66 Valli, J. *et al.* Seeing beyond the limit: A guide to choosing the right super-resolution microscopy technique. *The Journal of biological chemistry* **297**, 100791, doi:10.1016/j.jbc.2021.100791 (2021).
67 Lambert, T. J. & Waters, J. C. Navigating challenges in the application of superresolution microscopy. *Journal of Cell Biology* **216**, 53-63, doi:10.1083/jcb.201610011 (2016).
68 Lee, L. C.-C. & Lo, K. K.-W. Strategic Design of Luminescent Rhenium(I), Ruthenium(II), and Iridium(III) Complexes as Activity-Based Probes for Bioimaging and Biosensing. *Chemistry – An Asian Journal* **17**, e202200840, doi:https://doi.org/10.1002/asia.202200840 (2022).
69 Li, S.-H. *et al.* Emission Wavelength-Tunable Bicyclic Dioxetane Chemiluminescent Probes for Precise In Vitro and In Vivo Imaging. *Analytical Chemistry*, doi:10.1021/acs.analchem.3c02126 (2023).
70 Green, O. *et al.* Near-Infrared Dioxetane Luminophores with Direct Chemiluminescence Emission Mode. *Journal of the American Chemical Society* **139**, 13243-13248, doi:10.1021/jacs.7b08446 (2017).
71 Byrne, A., Burke, C. S. & Keyes, T. E. Precision targeted ruthenium(ii) luminophores; highly effective probes for cell imaging by stimulated emission depletion (STED) microscopy. *Chemical Science* **7**, 6551-6562, doi:10.1039/C6SC02588A (2016).
72 Baggaley, E. *et al.* Dinuclear Ruthenium(II) Complexes as Two-Photon, Time-Resolved Emission Microscopy Probes for Cellular DNA. *Angewandte Chemie International Edition* **53**, 3367-3371, doi:https://doi.org/10.1002/anie.201309427 (2014).
73 Sreedharan, S. *et al.* Multimodal Super-resolution Optical Microscopy Using a Transition-Metal-Based Probe Provides Unprecedented Capabilities for Imaging Both Nuclear

Chromatin and Mitochondria. *Journal of the American Chemical Society* **139**, 15907-15913, doi:10.1021/jacs.7b08772 (2017).

74 Smitten, K. L. *et al.* Using Nanoscopy To Probe the Biological Activity of Antimicrobial Leads That Display Potent Activity against Pathogenic, Multidrug Resistant, Gram-Negative Bacteria. *ACS Nano* **13**, 5133-5146, doi:10.1021/acsnano.8b08440 (2019).

75 Smitten, K. L. *et al.* Mononuclear ruthenium(II) theranostic complexes that function as broad-spectrum antimicrobials in therapeutically resistant pathogens through interaction with DNA. *Chemical Science* **11**, 8828-8838, doi:10.1039/D0SC03410J (2020).

76 Saeed, H. K. *et al.* Making the Right Link to Theranostics: The Photophysical and Biological Properties of Dinuclear Ru^{II}–Re^{I} dppz Complexes Depend on Their Tether. *Journal of the American Chemical Society* **142**, 1101-1111, doi:10.1021/jacs.9b12564 (2020).

77 Noakes, F. F. *et al.* Phenazine Cations as Anticancer Theranostics. *Journal of the American Chemical Society* **146**, 12836-12849, doi:10.1021/jacs.4c03491 (2024).

78 Jarman, P. J. *et al.* Exploring the Cytotoxicity, Uptake, Cellular Response, and Proteomics of Mono- and Dinuclear DNA Light-Switch Complexes. *Journal of the American Chemical Society* **141**, 2925-2937, doi:10.1021/jacs.8b09999 (2019).

79 Friedman, A. E., Chambron, J. C., Sauvage, J. P., Turro, N. J. & Barton, J. K. A molecular light switch for DNA: Ru(bpy)2(dppz)2+. *Journal of the American Chemical Society* **112**, 4960-4962, doi:10.1021/ja00168a052 (1990).

80 Chambron, J.-C. & Sauvage, J.-P. Ru (bipy)2dppz2+ : a highly sensitive luminescent probe for micellar sodium dodecyl sulfate solutions. *Chemical Physics Letters* **182**, 603-607, doi:https://doi.org/10.1016/0009-2614(91)90132-S (1991).

81 Dröge, F. *et al.* A Dinuclear Osmium(II) Complex Near-Infrared Nanoscopy Probe for Nuclear DNA. *Journal of the American Chemical Society* **143**, 20442-20453, doi:10.1021/jacs.1c10325 (2021).

82 Smitten, K. L., Scattergood, P. A., Kiker, C., Thomas, J. A. & Elliott, P. I. P. Triazole-based osmium(ii) complexes displaying red/near-IR luminescence: antimicrobial activity and super-resolution imaging. *Chemical Science* **11**, 8928-8935, doi:10.1039/D0SC03563G (2020).

83 Shaikh, S., Wang, Y., ur Rehman, F., Jiang, H. & Wang, X. Phosphorescent Ir (III) complexes as cellular staining agents for biomedical molecular imaging. *Coordination Chemistry Reviews* **416**, 213344, doi:https://doi.org/10.1016/j.ccr.2020.213344 (2020).

84 Mishra, P. & Chan, D. C. Mitochondrial dynamics and inheritance during cell division, development and disease. *Nature reviews. Molecular cell biology* **15**, 634-646, doi:10.1038/nrm3877 (2014).

85 Chen, Q. *et al.* Super-Resolution Tracking of Mitochondrial Dynamics with An Iridium(III) Luminophore. *Small* **14**, 1802166, doi:https://doi.org/10.1002/smll.201802166 (2018).

86 Friedman, J. R. & Nunnari, J. Mitochondrial form and function. *Nature* **505**, 335-343, doi:10.1038/nature12985 (2014).

87 de Boer, P., Hoogenboom, J. P. & Giepmans, B. N. Correlated light and electron microscopy: ultrastructure lights up! *Nat Methods* **12**, 503-513, doi:10.1038/nmeth.3400 (2015).

88 Tanner, H., Sherwin, O. & Verkade, P. Labelling strategies for correlative light electron microscopy. *Microscopy research and technique* **86**, 901-910, doi:10.1002/jemt.24304 (2023).

89 Shewring, J. R. *et al.* Multimodal Probes: Superresolution and Transmission Electron Microscopy Imaging of Mitochondria, and Oxygen Mapping of Cells, Using Small-Molecule

Ir(III) Luminescent Complexes. *Inorganic Chemistry* **56**, 15259-15270, doi:10.1021/acs.inorgchem.7b02633 (2017).

90 Tian, X. *et al.* A Cyclometalated Iridium (III) Complex as a Microtubule Probe for Correlative Super-Resolution Fluorescence and Electron Microscopy. *Advanced Materials* **32**, 2003901, doi:https://doi.org/10.1002/adma.202003901 (2020).

91 Liu, T. *et al.* An Iridium (III) complex revealing cytoskeleton nanostructures under super-resolution nanoscopy and liquid-phase electron microscopy. *Sensors and Actuators B: Chemical* **388**, 133839, doi:https://doi.org/10.1016/j.snb.2023.133839 (2023).

92 Huang, R. *et al.* Chiral Os(II) Polypyridyl Complexes as Enantioselective Nuclear DNA Imaging Agents Especially Suitable for Correlative High-Resolution Light and Electron Microscopy Studies. *ACS Applied Materials & Interfaces* **12**, 3465-3473, doi:10.1021/acsami.9b19776 (2020).

93 Huang, R. *et al.* Unprecedented enantio-selective live-cell mitochondrial DNA super-resolution imaging and photo-sensitizing by the chiral ruthenium polypyridyl DNA "light-switch". *Nucleic Acids Research* **51**, 11981-11998, doi:10.1093/nar/gkad799 (2023).

94 Dikova, Y. M., Yufit, D. S. & Williams, J. A. G. Platinum(IV) Complexes with Tridentate, NNC-Coordinating Ligands: Synthesis, Structures, and Luminescence. *Inorganic Chemistry* **62**, 1306-1322, doi:10.1021/acs.inorgchem.2c04116 (2023).

95 Chaaban, M., Zhou, C., Lin, H., Chyi, B. & Ma, B. Platinum(ii) binuclear complexes: molecular structures, photophysical properties, and applications. *Journal of Materials Chemistry C* **7**, 5910-5924, doi:10.1039/C9TC01585J (2019).

96 Mauro, M., Aliprandi, A., Septiadi, D., Kehr, N. S. & De Cola, L. When self-assembly meets biology: luminescent platinum complexes for imaging applications. *Chemical Society Reviews* **43**, 4144-4166, doi:10.1039/C3CS60453E (2014).

97 Johnstone, T. C., Suntharalingam, K. & Lippard, S. J. The Next Generation of Platinum Drugs: Targeted Pt(II) Agents, Nanoparticle Delivery, and Pt(IV) Prodrugs. *Chemical Reviews* **116**, 3436-3486, doi:10.1021/acs.chemrev.5b00597 (2016).

98 Liu, L.-Y. *et al.* Multiple-Color Platinum Complex with Super-Large Stokes Shift for Super-Resolution Imaging of Autolysosome Escape. *Angewandte Chemie International Edition* **59**, 19229-19236, doi:https://doi.org/10.1002/anie.202007878 (2020).

99 Shen, Y. *et al.* Visualization of mitochondrial DNA in living cells with super-resolution microscopy using thiophene-based terpyridine Zn(ii) complexes. *Chemical Communications* **54**, 11288-11291, doi:10.1039/C8CC06276E (2018).

100 Liu, D. H., Sun, Z. B., Zhao, Z. H., Peng, Q. & Zhao, C. H. 1,1'-Binaphthyl Consisting of Two Donor-π-Acceptor Subunits: A General Skeleton for Temperature-Dependent Dual Fluorescence. *Chemistry (Weinheim an der Bergstrasse, Germany)* **25**, 10179-10187, doi:10.1002/chem.201901719 (2019).

101 Du, W. *et al.* Terpyridine Zn(II) Complexes with Azide Units for Visualization of Histone Deacetylation in Living Cells under STED Nanoscopy. *ACS Sensors* **6**, 3978-3984, doi:10.1021/acssensors.1c01287 (2021).

102 Tian, X. *et al.* A combination of super-resolution fluorescence and magnetic resonance imaging using a Mn(ii) compound. *Inorganic Chemistry Frontiers* **6**, 2914-2920, doi:10.1039/C9QI00895K (2019).

103 Mallik, R. *et al.* Folate Receptor Targeting Mn(II) Complex Encapsulated Porous Silica Nanoparticle as an MRI Contrast Agent for Early-State Detection of Cancer. *Small* **n/a**, 2401787, doi:https://doi.org/10.1002/smll.202401787.

104 Liu, J. *et al.* Nucleolar RNA in action: Ultrastructure revealed during protein translation through a terpyridyl manganese(II) complex. *Biosensors and Bioelectronics* **203**, 114058, doi:https://doi.org/10.1016/j.bios.2022.114058 (2022).
105 Bastide, A., Yewdell, J. W. & David, A. The RiboPuromycylation Method (RPM): an Immunofluorescence Technique to Map Translation Sites at the Sub-cellular Level. *Bio-protocol* **8**, doi:10.21769/BioProtoc.2669 (2018).
106 Balzarotti, F. *et al.* Nanometer resolution imaging and tracking of fluorescent molecules with minimal photon fluxes. *Science* **355**, 606-612, doi:10.1126/science.aak9913 (2017).
107 Gwosch, K. C. *et al.* MINFLUX nanoscopy delivers 3D multicolor nanometer resolution in cells. *Nature Methods* **17**, 217-224, doi:10.1038/s41592-019-0688-0 (2020).
108 Schmidt, R. *et al.* MINFLUX nanometer-scale 3D imaging and microsecond-range tracking on a common fluorescence microscope. *Nature Communications* **12**, 1478, doi:10.1038/s41467-021-21652-z (2021).
109 Prakash, K. At the molecular resolution with MINFLUX? *Philosophical Transactions of the Royal Society A: Mathematical, Physical and Engineering Sciences* **380**, 20200145, doi:doi:10.1098/rsta.2020.0145 (2022).
110 van de Linde, S., Heilemann, M. & Sauer, M. Live-cell super-resolution imaging with synthetic fluorophores. *Annual review of physical chemistry* **63**, 519-540, doi:10.1146/annurev-physchem-032811-112012 (2012).
111 Rust, M. J., Bates, M. & Zhuang, X. Sub-diffraction-limit imaging by stochastic optical reconstruction microscopy (STORM). *Nature Methods* **3**, 793-796, doi:10.1038/nmeth929 (2006).
112 Huang, B., Wang, W., Bates, M. & Zhuang, X. Three-dimensional super-resolution imaging by stochastic optical reconstruction microscopy. *Science* **319**, 810-813, doi:10.1126/science.1153529 (2008).
113 Huang, B., Jones, S. A., Brandenburg, B. & Zhuang, X. Whole-cell 3D STORM reveals interactions between cellular structures with nanometer-scale resolution. *Nature Methods* **5**, 1047-1052, doi:10.1038/nmeth.1274 (2008).
114 Betzig, E. *et al.* Imaging intracellular fluorescent proteins at nanometer resolution. *Science* **313**, 1642-1645, doi:10.1126/science.1127344 (2006).
115 Tang, J. *et al.* A photoactivatable Znsalen complex for super-resolution imaging of mitochondria in living cells. *Chemical Communications* **52**, 11583-11586, doi:10.1039/C6CC06531G (2016).

[H1] References to be highlighted and short descriptions why.

71. Byrne, A.; Burke, C. S.; Keyes, T. E., Precision targeted ruthenium(ii) luminophores; highly effective probes for cell imaging by stimulated emission depletion (STED) microscopy. *Chemical Science* 2016, *7* (10), 6551-6562.
This first report to investigate the potential of metal complexes for STED microscopy; also demonstrating how they could be appended with established targeting peptide to drive sub-cellular location of such imaging agents

73. Sreedharan, S.; Gill, M. R.; Garcia, E.; Saeed, H. K.; Robinson, D.; Byrne, A.; Cadby, A.; Keyes, T. E.; Smythe, C.; Pellett, P.; Bernardino de la Serna, J.; Thomas, J. A., Multimodal Super-resolution Optical Microscopy Using a Transition-Metal-Based Probe Provides Unprecedented Capabilities for Imaging Both Nuclear Chromatin and Mitochondria. *Journal of the American Chemical Society* **2017,** *139* (44), 15907-15913

This highly photostable, cell permeant complex with a large Stokes shift was found to be a multimodal probe that can be used for imaging of mitochondria and nuclear chromatin by SIM, STED and 3D-STED in both fixed and live cells, as well as a TEM contrast stain.

74. Smitten, K. L.; Southam, H. M.; de la Serna, J. B.; Gill, M. R.; Jarman, P. J.; Smythe, C. G. W.; Poole, R. K.; Thomas, J. A., Using Nanoscopy To Probe the Biological Activity of Antimicrobial Leads That Display Potent Activity against Pathogenic, Multidrug-Resistant, Gram-Negative Bacteria. *ACS Nano* **2019,** *13* (5), 5133-5146.

The first such investigation in prokaryotes illustrated how the inherent SRM properties of metal complex-based antimicrobial therapeutic leads could be used to probe their mechanism of action against resistant pathogens by directly imaging intracellular targets.

85. Chen, Q.; Jin, C.; Shao, X.; Guan, R.; Tian, Z.; Wang, C.; Liu, F.; Ling, P.; Guan, J.-L.; Ji, L.; Wang, F.; Chao, H.; Diao, J., Super-Resolution Tracking of Mitochondrial Dynamics with An Iridium(III) Luminophore. *Small* **2018**, *14* (41), 180216.

In this study, the low photobleaching and overall photostability of Iridium(III)-based probe allowed detailed investigations into mitochondria and lysosomes and their interactions in different conditions to be investigated using SIM.

90. Tian, X.; De Pace, C.; Ruiz-Perez, L.; Chen, B.; Su, R.; Zhang, M.; Zhang, R.; Zhang, Q.; Wang, Q.; Zhou, H.; Wu, J.; Zhang, Z.; Tian, Y.; Battaglia, G., A Cyclometalated Iridium (III) Complex as a Microtubule Probe for Correlative Super-Resolution Fluorescence and Electron Microscopy. *Advanced Materials* **2020**, *32* (39), 2003901.

The first example of a single molecule probe suitable for CLEM involving both SRM (STED) and TEM.

102. Tian, X.; Xiao, L.; Shen, Y.; Luo, L.; Zhang, G.; Zhang, Q.; Li, D.; Wu, J.; Wu, Z.; Zhang, Z.; Tian, Y., A combination of super-resolution fluorescence and magnetic resonance imaging using a Mn(ii) compound. *Inorganic Chemistry Frontiers* 2019, *6* (10), 2914-2920.

A study that employs an Earth-abundant first-row transition metal ion in a SRM probe that is also MRI active, providing potential to image across a wide range of scales

115. Tang, J.; Zhang, M.; Yin, H. Y.; Jing, J.; Xie, D.; Xu, P.; Zhang, J. L. A Photoactivatable Znsalen Complex for Super-Resolution Imaging of Mitochondria in Living Cells. *Chem. Commun.* 2016, *52*, 11583–11586.

This report on a Zinc(II)-based probe for STORM demonstrates that the luminescent properties of metal complexes can be compatible with stochastic SRM techniques.

[H1] Graphical abstract

Suggested ToC GA (we can supply at right size):

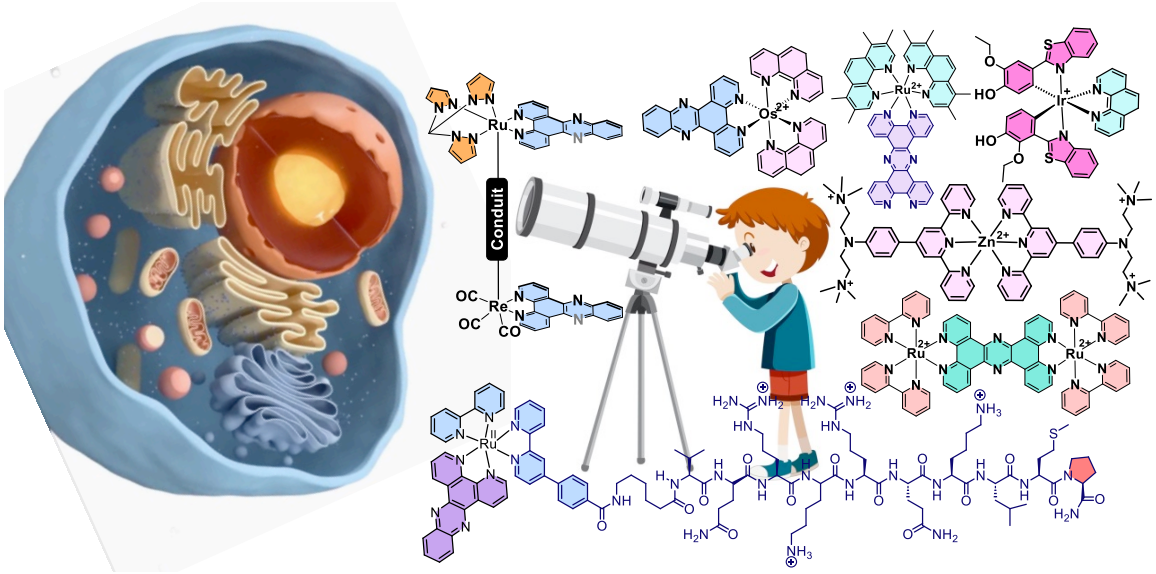

[H1] ToC blurb

Suggested blurb:

Super-resolution microscopy techniques can break conventional optical diffraction limits, but their performance can only be optimized by using probes with appropriate biophysical and photophysical properties. This review highlights how transition-metal complexes are being designed to meet these challenges.